TECHNICAL REPORT

SPACE
TELESCOPE
SCIENCE
INSTITUTE

Operated for NASA by AURA

Title: Simulations of Target Acquisition with MIRI Four-Quadrant Phase Mask Coronagraph (II).	Doc #: JWST-STScI-003065, SM-12 Date: September 26 2012 Rev: -
Authors: Charles-Philippe Lajoie, Rémi Soummer, Dean Hines Phone: 410 - 338 - 5007	Release Date: 13 February 2013

1   Abstract

We present the results of the second part of a comprehensive study on target acquisition with JWST's Mid-Infrared Instrument (MIRI) four-quadrant phase mask (4QPM) coronagraph using numerical simulations (see Soummer et al. 2012; paper I hereafter). The adverse effects of the coronagraph and the observatory's slew accuracy on target acquisition are known to limit our ability to position stars at the center of the coronagraph. Here, we investigate further these two effects and use different scenarios involving single and multiples   acquisitions to mitigate them. We also investigate the effects of wavelength, wavefront error, latency, intermediate distances, and detector noise on the different scenarios' performances. Unlike the intermediate position, we find that latency and noise do not affect TA significantly. We also find that scenarios that require fewer acquisitions yield final pointings with smaller dispersions but larger offsets, and vice versa. At this point, we estimate that a single acquisition at 500 mas from the center of the coronagraph constitutes our best approach for TA with MIRI four-quadrant phase mask coronagraph.

2   Introduction

Coronagraphic capabilities on the Mid-Infrared Instrument (MIRI) will be achieved using a classical Lyot mask optimized at 23 µm as well as three four-quadrant phase masks (4QPMs) optimized at 10.65, 11.40, and 15.50 µm. In theory, a 4QPM allows for complete cancellation of on-axis light and its smaller inner working angle also allows for detection of disk, planets, and debris disks closer to the central object. However, for optimal contrast and performance, the target object has to be positioned as close to the center of the 4QPM as possible (10 mas radial requirement) and the reference star is to be found within 5 mas from the target. These requirements are difficult to meet because (1) the observatory has a limited slew accuracy, (2) the 4QPM induces a non-linear distortion of the PSF, (3) the position of the center of the 4QPM is not known exactly (to within 1-2 mas). The distortion induced by the 4QPM effectively limits our ability to pinpoint the position of the stars and therefore makes Target Acquisition (TA) on MIRI using the 4QPM challenging. It is therefore imperative that a strategy to minimize these adverse effects is developed.

In this report, we investigate the combined effects of the 4QPM, the slew accuracy, and scenarios in order to determine the optimal procedure for TA with MIRI 4QPM. We first present our computational method and approach in §3. We present and discuss our results at 11.40 µm along

Check with the JWST SOCCER Database at: https://soccer.stsci.edu
to verify that this is the current version.

with the various ingredients we incorporated in §4. In §5 and §6 we discuss the different scenarios used and the TA investigation at 15.50 µm, respectively. Finally, in §7 we discuss the potential use of the second and third centroid moments, and our main conclusions and recommendations are summarized in §8.

3   Computational Method and Approach

To optimize the TA procedure, we use numerical simulations of coronagraphic images using an updated version of the code presented and thoroughly tested in paper I and in Soummer & Makidon (2010). This code propagates the electric field from the pupil plane to the focal plane and incorporates different intervening masks, filters, and Lyot stops as well as realistic transmission profiles for the neutral density filter (FND)[1] and the 4QPM's Germanium coating. Centroid measurement is done using the same Floating Window algorithm (Meixner et al. 2007 and references therein) that will be integrated onboard the observatory. Our simulations include a detailed model of the errors on centroid from the coronagraphs mask, but assume that there is no additional drift of the pointing system during the TA process.
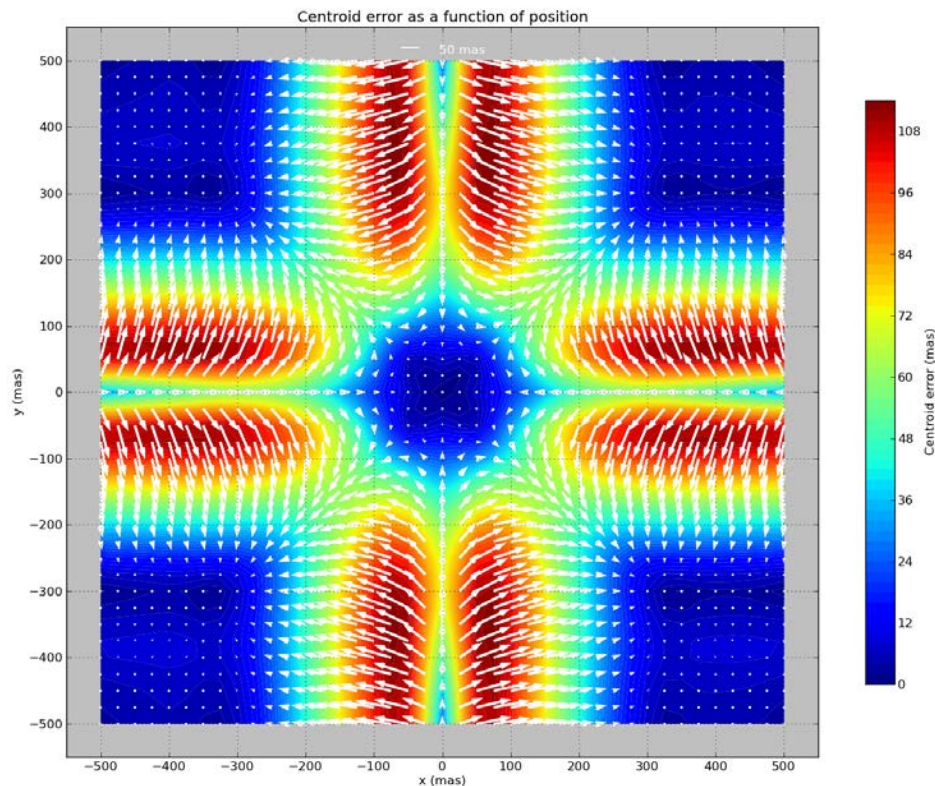
Figure 1 Centroid error as a function of position on the $QPM at 11.4 µm without wavefront error. The vectors point from the true position to the actual centroid (measured) position. See also Figures 4 and 5 in paper I for a one-dimensional representation of this map.

---

[1] The attenuation of the FND is ~ 2×10^{-3}.

In our simulations, the masks are fixed and the target can be positioned anywhere with respect to the center of the 4QPM. However, two ingredients in our simulations limit our ability to position (and know exactly the position of) the star at the center of the 4QPM: the effects of the coronagraph on the PSF and the observatory's slew accuracy. **Error! Reference source not found.** shows the error on the centroid measurement as a function of position on the 4QPM and demonstrates (1) that the 4QPM can introduce errors as large as 100 mas on the centroid measurement depending on the position of the star relative to the 4QPM center and (2) that one should avoid the axes of the 4QPM and aim for regions with the smallest errors (see also paper I).
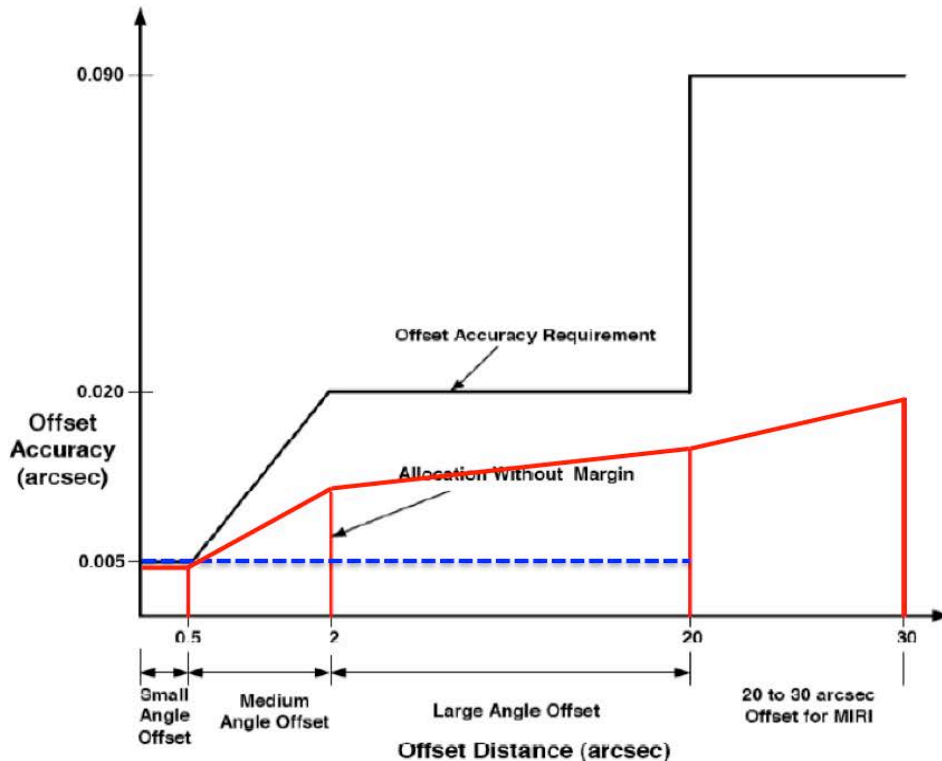
Figure 2 Slew accuracy as a function of slew size. In this report, we use different slew accuracies to estimate the contribution of slew accuracy to our final pointings. Requirement (*black*), Expected (*red*) and CDR (newest *blue*)

Also, it is interesting to note the symmetrical nature of **Error! Reference source not found.**, which we will try to exploit in §5. **Error! Reference source not found.**, on the other hand, shows the different slew accuracy models predicted for the future observatory. Note that the requirement model has a larger error for larger slews whereas the JWST Critical Design Review (CDR) model remains constant all the way out to 20". The Expected model (red curve) is an intermediate, earlier model of the slew accuracy and is also used for comparison. We emphasize here that these curves are based on models and that the true slew accuracy will not be known until commissioning. Finally, we also consider the case of currently proposed slews under fine guidance using the Fine-Steering Mirror (FSM; 1 mas 1-σ per axis) for slews smaller than 50 mas.

We note however that there is no implementation of such slew mode at the moment in the current flight software, although a request has been put forward.

To circumvent some of the difficulties imposed by the 4QPM as well as by the limited slew accuracy, we simulate TA using different scenarios, all shown in Figure 3. All the scenarios use the same starting position (5") and various intermediate positions are used (ranging from 4" to 150 mas).
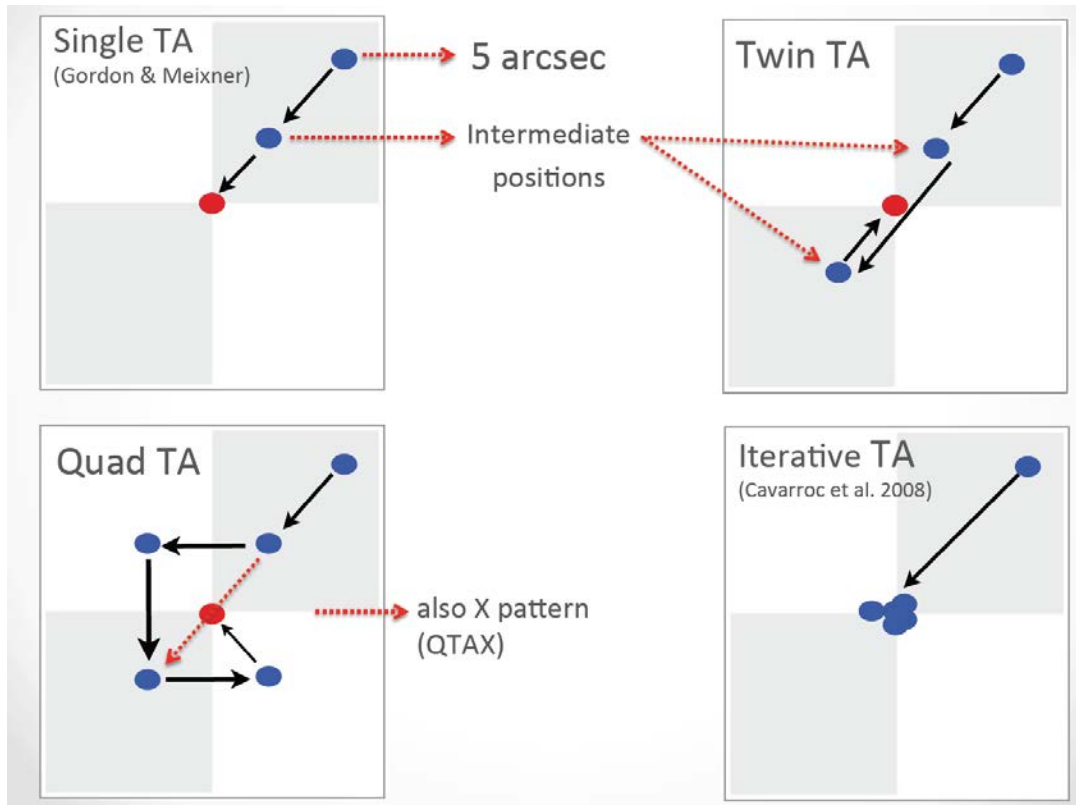
Figure 3 Different TA scenarios used in our simulations

We use scenarios involving multiple intermediate acquisitions to assess whether the symmetrical distortion of the 4QPM can be averaged and cancelled out. We also enforce that all scenarios stay away from the axes of the 4QPM, since the centroid measurement error is largest there (see **Error! Reference source not found.**).   The centroid measurements are averaged and used to make the final slew to the center of the 4QPM. Unlike the other scenarios, the Iterative TA scenario (see Cavarroc et al. 2008) aims for the center straight from 5" and then iterates towards the center of the 4QPM until convergence is achieved. Under the Iterative TA scenario, we can also use the FSM slew accuracy model, as described above, since most slews are smaller than 50 mas. This is discussed further in §5.

Finally, because of the random nature of the pointing errors in the slew models, we run multiple (generally 50) realizations of TA using the same simulation parameters and then determine the dispersion and offset of all the final pointings. We use these values to assess the accuracy and repeatability of a given scenario.

4   Preliminary Results at 11.40 μm

The lower-left panel of Figure 4 illustrates typical results from our TA simulations, where the standard deviation and offsets from the mean are also reported. Each dot represents the final pointing of a realization under the TA scenario used (in this case, Single TA) and the red circles delimitate the 1- and 2-σ radii from the mean offset. The histograms show the distributions of final pointings in x, y, and radius along with the 1- and 2-σ markers (dashed lines). All values are in milliarcseconds, unless otherwise noted, and performances of each scenario are assessed based on these derived values.
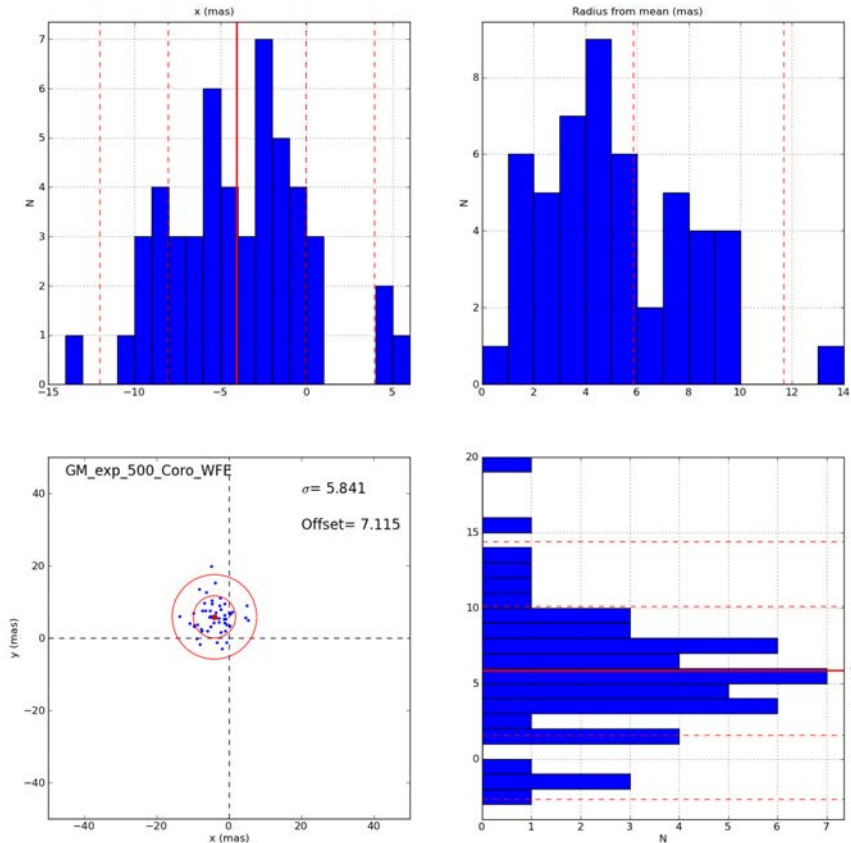
Figure 4 Typical Results from one of the simulations with 50 realizations for the 11.40 μm 4QPM. This particular case used the Single TA scenario (GM), the Expected slew accuracy model (exp) and an intermediate position of 500 mas.

Although not shown in this work, we have also run simulations with and without wavefront error (WFE) or the coronagraph to disentangle their effects on the final pointings. In general, when compared to a telescope with "perfect" optics (but still with slew error), we note that the dispersion increases by a few percent when including the WFE and/or the coronagraph. We shall not discuss further these preliminary simulations here. Next, we discuss the separate effects of changing the WFE, the intermediate position, the latency, and noise on final pointings.

4.1   Effect of Wavefront Error

The effect of changing the WFE in our simulations is subtle but not insignificant, as can be seen in **Error! Reference source not found.**.
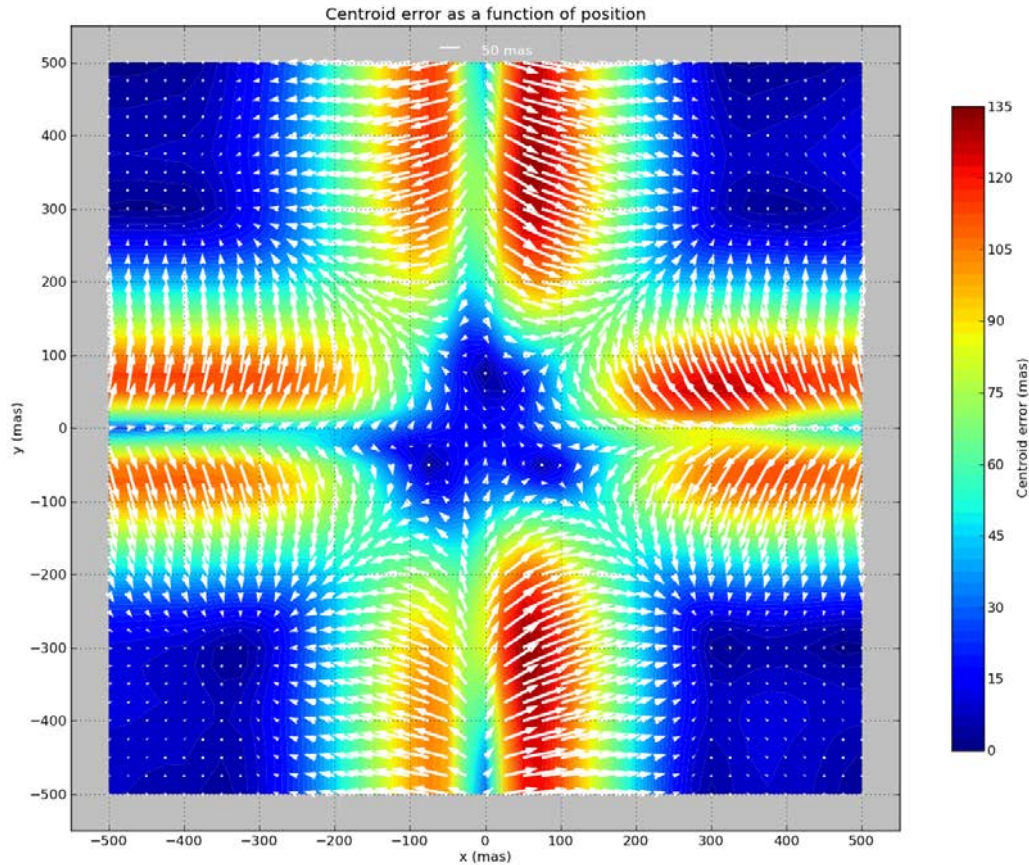
Figure 5 Centroid error as a function of position on the 4QPM at 11.4 μm with wavefront error. The vectors point from the true position to the actual centroid (measured) position.

Again, the largest errors on the centroid measurement are found close the axes, and WFE only slightly changes the overall pattern when compared to **Error! Reference source not found.**. The overall symmetry is maintained, although in this particular case, the maximum error reache ~135 mas whereas the centroid error within 50 mas of the center of the 4QPM is about 10-15 mas. **Error! Reference source not found.**, on the other hand, shows the effect of changing the WFE on the final pointings, where we used different WFE maps (Rev. V). The main consequence of changing the WFE is, apart from a small change in dispersion of ~5%, a random shift in the mean offset. These small variations, along with the fact that the WFE will change regularly during commissioning and science operations (every two weeks), will likely prevent the use of such a map to help calibrate TA.
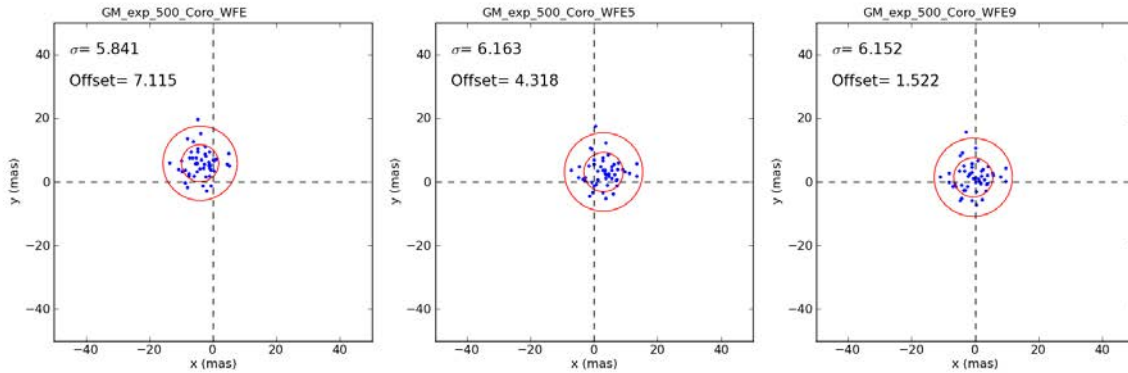
Figure 6 Effect of using different wavefront error maps on the final pointings for the Single TA scenario and the Expected slew accuracy model.

4.2 Effect of Latency

Electronic residuals on the detector from previous acquisition images can potentially interfere with the centroid measurement algorithm and further limit the accuracy of any TA procedure. To investigate the effect of latent images, we include it in our simulations for scenarios that involve multiple intermediate acquisitions only, i.e. Twin TA and Quad TA. We note however that we did not run the Iterative TA scenario with latency. Latency on the MIRI infrared detector can usually be characterized with an exponential decay of the original image with a folding time of ~300 seconds (G.Rieke, priv. comm.). Here, we use a simpler approach: for a given latency fraction (from 0 to 20%), we imprint that fraction of the preceding intermediate image onto the next image before performing centroid measurement.
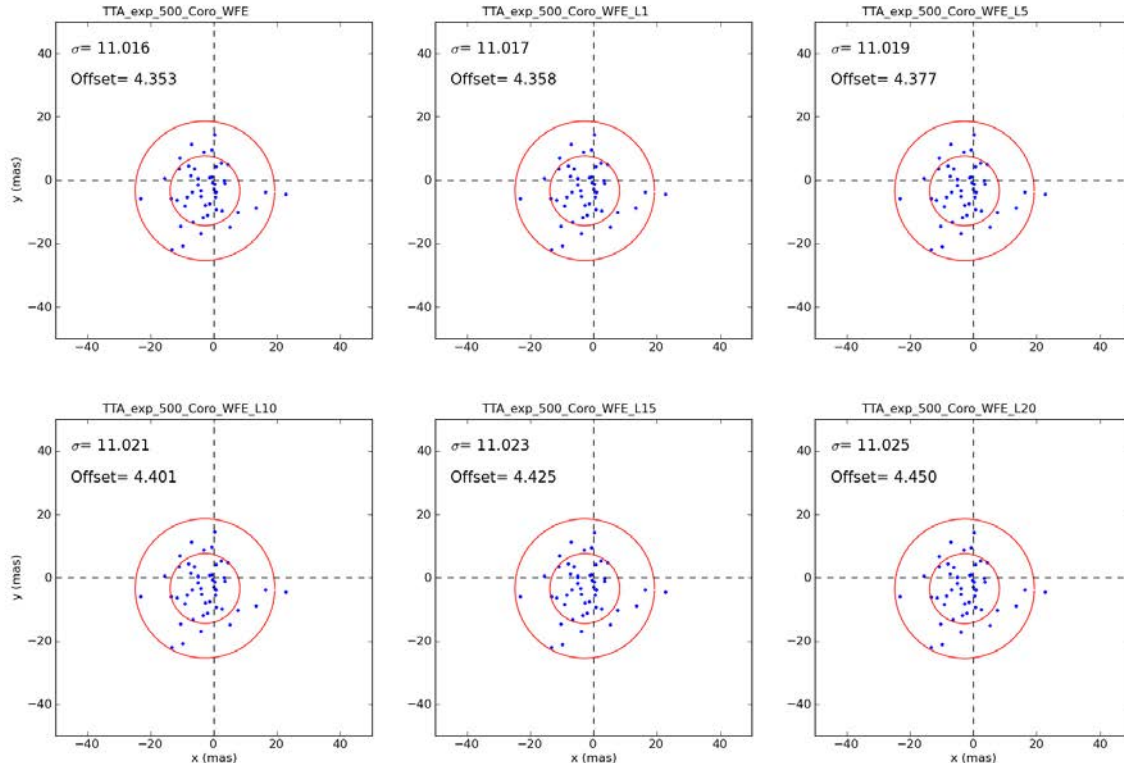
Figure 7 Effect of latency on the final pointings for the Twin TA scenario under the Expected slew accuracy model. From the left to right, the latency is 0, 1 and 5% (top row) and 10, 15 and 20% (bottom row).

Figure 7 shows latency tests performed with the Twin TA scenario for various latency fractions, ranging from 0 to 20%. It is clear that latency, even up to 20%, does not affect TA. The final pointings dispersion does not change significantly and the mean offset shifts by no more than ~2%. Even if latency does not affect TA, it might impact faint science images. Therefore, we must ensure that TA is performed far enough from the center of the 4QPM, keeping in mind that the PSF FWHM at 10.65 and 15.50 μm is about 300 and 500 mas respectively. We investigate the effect of changing the intermediate position next.

4.3   Effect of Intermediate Position

The effect of changing the intermediate position during TA is much more important than the WFE or latency, as can be seen in **Error! Reference source not found.**. Using the Single TA scenario and intermediate positions of 1000, 750, 500, and 150 mas (from left to right), we see two important effects: (1) as we slew to the center from smaller distances, the slew uncertainty gets smaller and therefore tightens the final pointings; (2) as we get too close to the center of the 4QPM, the distortion of the PSF becomes such that error on the centroid measurement throws the star off the center by more than 50 mas in some cases (see also **Error! Reference source not found.**). Given the slew accuracy model used, **Error! Reference source not found.** demonstrates the importance of using small slews of ~500 mas (for which the uncertainty is ~5 mas 1-σ per-axis).
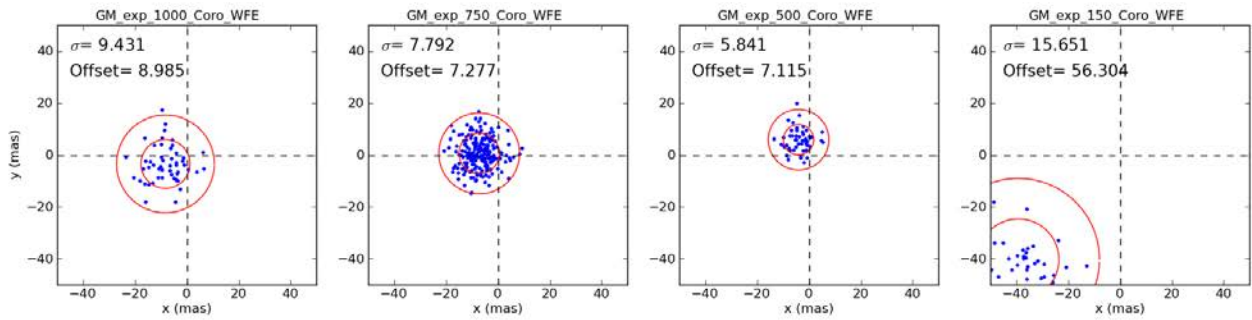
Figure 8 Effect of intermediate position on the final pointings for the Single TA scenario and the Expected slew accuracy model. From left to right, the intermediate positions are 1000, 750, 500 and 150 mas.

We also investigate cases where the intermediate position extends out to 4 arc seconds, i.e. beyond the angular size of the PSF (~350-500 mas radius depending on the wavelength). These cases are interesting because they limit significantly the potential contribution of latent images on the *science* image at the center of the 4QPM.

Error! Reference source not found. shows typical results for the Single TA scenario, different slew models, and various intermediate positions. The panels on the top row of **Error! Reference source not found.** all use the Requirement slew accuracy model and we see that the further out we go, the larger the final dispersion gets, similarly to **Error! Reference source not found.**. This is a direct consequence of the increasing error on the slew for larger slews (see **Error! Reference source not found.**). On the other hand, the panels on the bottom row of **Error! Reference source not found.** use the CDR slew accuracy model and show a more or less constant dispersion, a consequence of the constant error of this model. In this case, larger slews do not impact the dispersion of the final pointings although, interestingly, the mean offsets are observed to be smaller than at 500 mas in some cases. The fact that the dispersion is not affected by the larger slews (with the CDR model) is interesting since it could allow for TA to be performed further away from the science images, therefore decreasing the effect of latency on the latters. However, even with the CDR model, intermediate positions smaller than ~500 mas still suffer from being too close to the center of the 4QPM. Although the results using the CDR slew accuracy model are encouraging, the slew accuracy will be know only during commissioning.
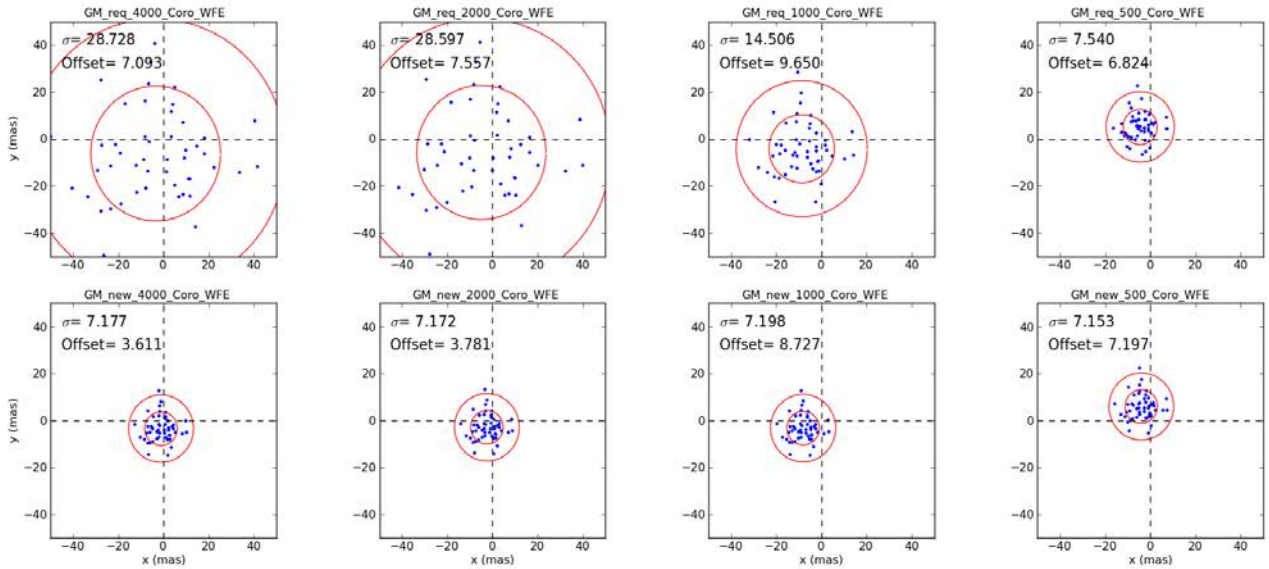
Figure 9 Effect of larger intermediate position on the final pointings for the Single TA scenario and the Requirement (*top row*) and CDR (*bottom row*) slew accuracy models. From left to right, the intermediate positions are 4000, 2000, 1000 and 500 mas.

4.4   Effect of Detector, Photon, and Background Noise

We now discuss the effect of noise on TA. Here, we follow the procedure outlined in Cavarroc et al. (2008) and we include photon, background, and readout noise sources. This noise is added to our images before every centroid measurement is performed.
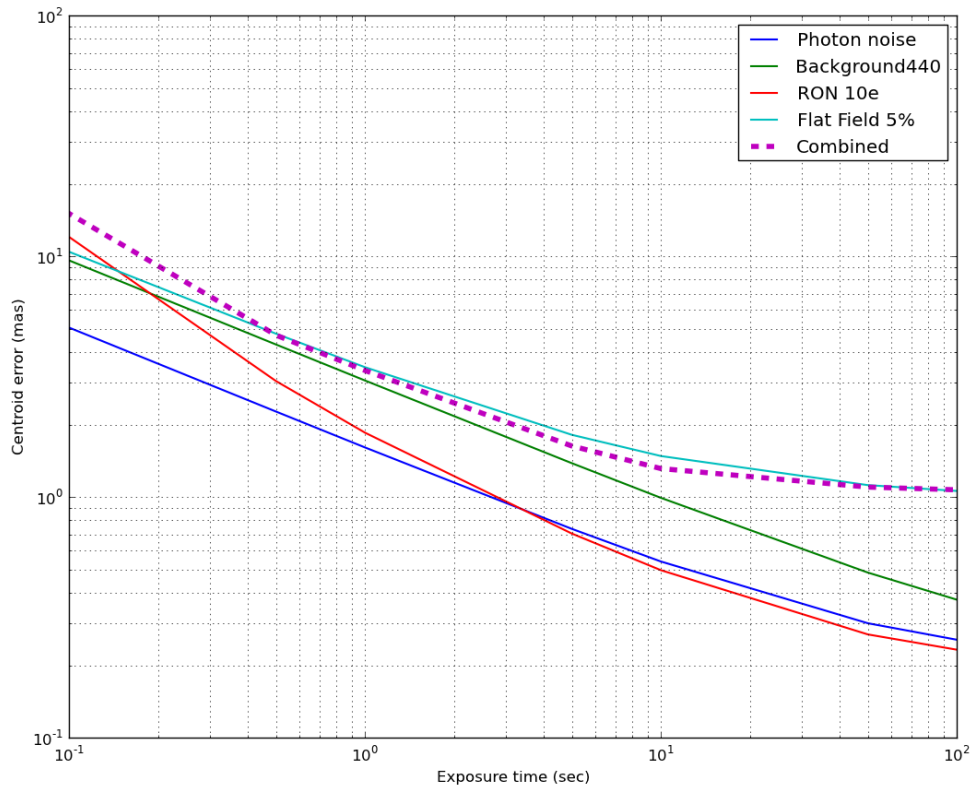
Figure 10 Error on the centroid measurement given different sources of noise. Note that we remove the bias, which is error on the centroid measurement when neither noise nor the 4QPM are used. The bias is typically ~0.5 mas radial.

To model noise, we use a Solar spectrum, scaled at 10 pc, and integrate it over a specified number of wavelength bands. We propagate each wavelength in our code through the 4QPM as well as the FND, the 4QPM Germanium transmission, and the quantum efficiency. Following Cavarroc et al. (2008), we also include a background noise of 440 electrons per pixel per second, which includes contributions from the zodiacal light as well as the mirrors, sunshield, and the instrument itself.

Figure 10 shows the behaviour of the centroid measurement error as a function of the exposure time (equivalently, the number of incident photons reaching the detector) for the various noise sources. The curves on Figure 10 are derived by calculating a coronagraphic image centered on the 4QPM, adding noise to it, and then measuring the centroid and the error on it. Given the random nature of the photon and background noise, we perform 100 centroid measurements and average the error. For short exposures, the error is dominated by the readout noise, whereas flat field deffects dominate at longer exposures. We also see in **Error! Reference source not found.** that the centroid error levels off around 1 mas radial for exposure times longer than ~10 seconds. These results suggest that we should not expect these noise sources to significantly impact TA. We also note that our results are consistent with those of Cavarroc et al. (2008).

For the TA simulations reported in **Error! Reference source not found.**, we use a readout noise of 10 electrons, a flat field variation of 5%, and an exposure time of 1 second for our Solar-like

model. The simulations are done in exactly the same manner as discussed above, with the addition of noise prior to performing every centroid measurement. **Error! Reference source not found.** compares the same sets of simulations with and without noise. Our results show that the addition of noise does not impact the target acquisition significantly, as expected. Indeed, the dispersion changes by no more than ~8% (Quad TA X) and the mean offset drifts in no particular direction around the center of the 4QPM.
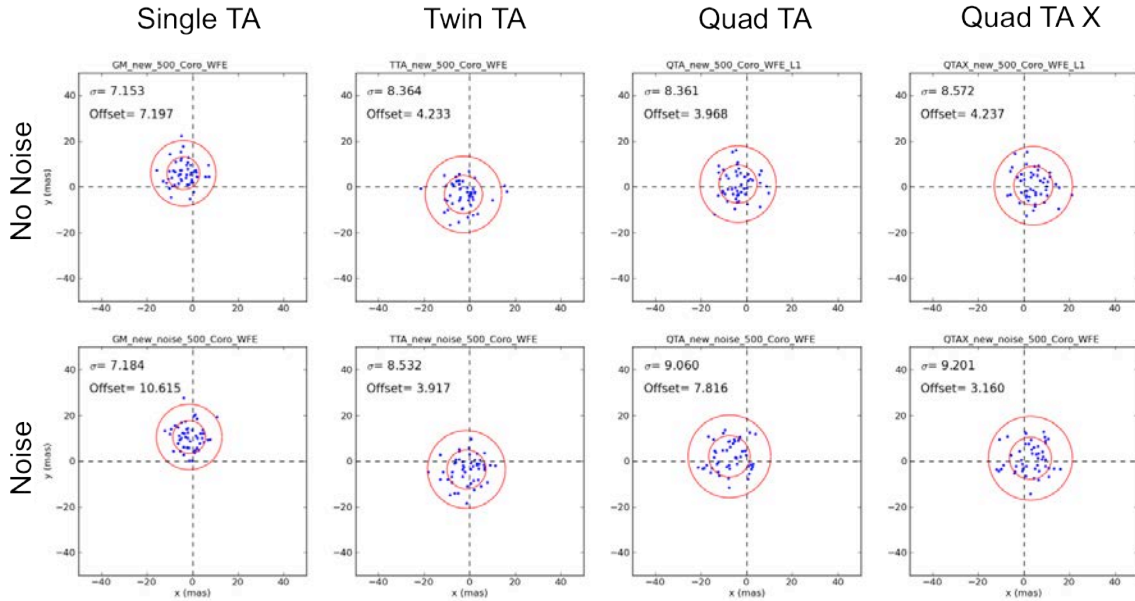
Figure 11: Comparison of final pointings without (*top row*) and with (*bottom row*) photon and detector noise using the CDR slew accuracy model. The different models are, from left to right, Single TA, Twin TA, Quad TA and Quad TA X.

5   Performances of the Different Scenarios

We now discuss the relative performances of the different scenarios used in our simulations (e.g. **Error! Reference source not found.**). In particular, we are interested not only in the tightness and offset of the final pointings but also in the number of acquisitions required to achieve a level of pointing accuracy. In §§4.2 and 4.4, we showed that latency and noise do not affect TA, so we do not include them in the following simulations and discussion, unless otherwise noted. We do however always add WFE map as well as the 11.40 μm 4QPM.

5.1   Iterative TA

The Iterative TA scenario consists in moving the star from 5 arcseconds out straight to the center and iterating its position until convergence (i.e. as close to the center of the 4QPM as possible) is reached. Our convergence criterion is set to 10 mas, which is the requirement for the science target. We limit the number of iterations to six here, however, for performance reasons. **Error! Reference source not found.** (*top panel*) shows the results for the CDR slew accuracy model, which converges the most rapidly because of its smaller inherent slew error. The leftmost panel shows that out of 50 realizations, 42 make it within 10 mas on any of the six iterations. The

histogram shows that all of the iterations that converge made it on the first iteration. Because of the error on the centroid so close to the 4QPM, any subsequent iteration results in an outward drift, with some realizations sometimes coming within 10 mas again. More importantly, the histogram shows that the realizations that did not converge on the first iteration do not converge during any other iteration, demonstrating that there is no benefit in iterating more than once with the CDR model. Moreover, the rightmost panels show that the mean offset slowly drifts out as we keep iterating, whereas the dispersion increases by ~15%. Clearly, based on **Error! Reference source not found.**, we conclude that iterating the position of the star (when within 50 mas of the center of the 4QPM) does not improve the pointings performances of the coronagraph.

As mentioned in §3, we also make use of the FSM slew potential capability for slews smaller than 50 mas, although this slew mode is not yet implemented in flight software. This mode is adequate for the Iterative scenario since all of the iterations are performed when within ~30-40 mas from the center of the 4QPM. **Error! Reference source not found.** (*bottom panel*) shows the results of the Iterative scenario with FSM slews, where the effect of higher-accuracy FSM slews is obvious. Indeed, the results are much tighter (factor ~4) for the second and third iterations, although the mean offsets are similarly large. The reason for such a tight dispersion is the small slew error associated with FSM steering. The large offset, on the other hand, is due to the fact that the centroid position and the actual telescope pointing are largely offset because of the distortion caused by the 4QPM and that we do not know exactly where the star really is.
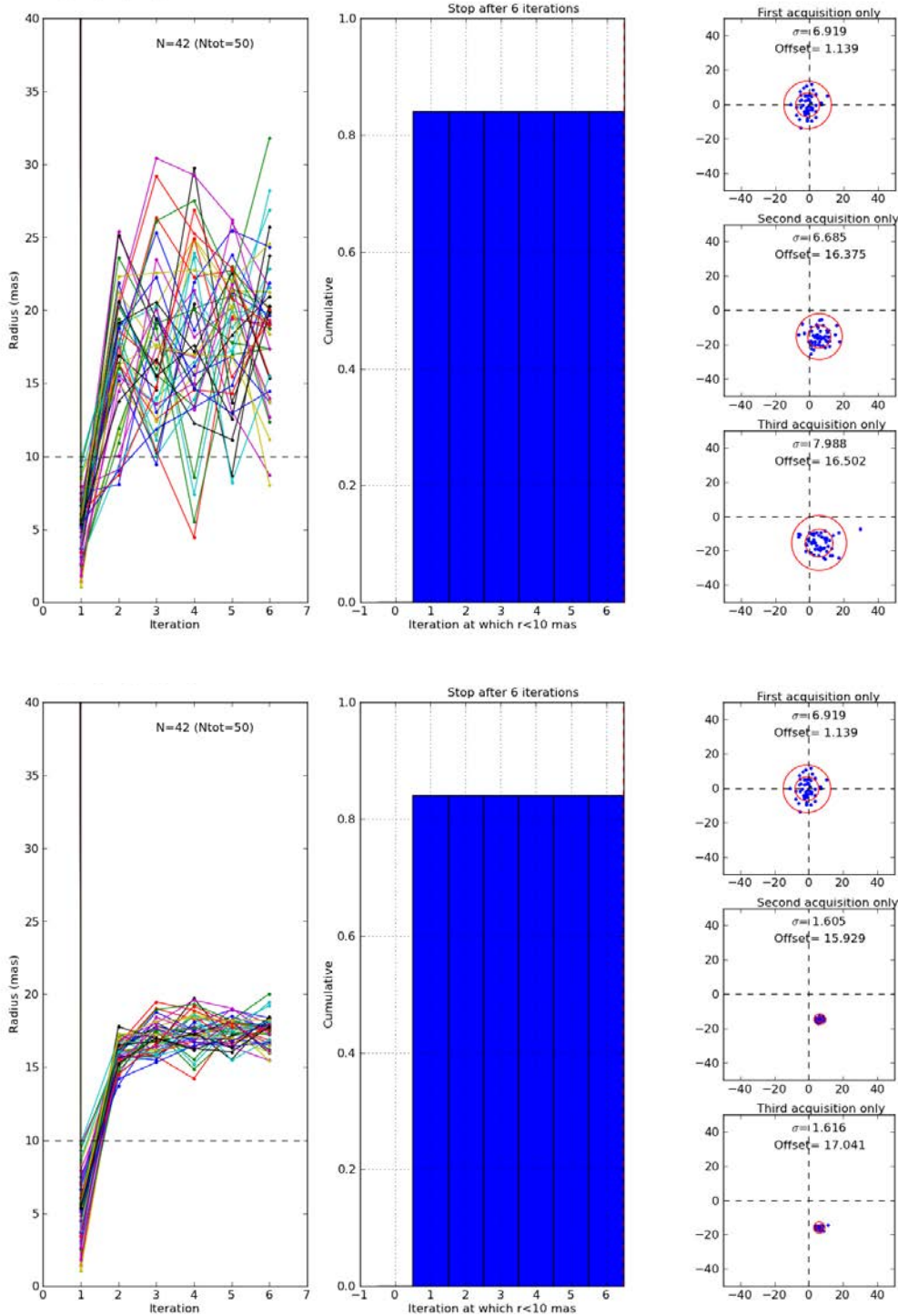
Figure 12 Iterative TA scenario results for the CDR (top) and CDR+FSM (bottom) slew models. Left: Radial distance from the center of the 4QPM as a function of iteration for the realizations that converged at one point during the iterations. Middle: Cumulative fraction of iterations converging as a function of iteration. Right: Final pointings as a function of the iteration.

Since we use the centroid to calculate the next slew (and *not* the telescope pointing), the latter ends up being consistently off. The tight dispersion seen in the bottom panel of **Error! Reference source not found.** is unmatched (when compared to other scenarios; see below) and therefore offers the possibility of calibrating this offset. We must be careful however as this offset is likely sensitive to WFE and therefore might change during commissioning and regular maintenance. The Iterative TA simulations shown here again emphasize that the final pointings dispersion is very sensitive on the slew accuracy model used.

5.2   Single TA

The Single TA scenario (Gordon & Meixner 2008) relies on only one intermediate acquisition, which limits the error introduced by multiple slews. Figure 13 shows the simulation results for both the Requirement and the CDR slew accuracy models (top and bottom rows respectively). Again, we see that getting too close to the center of the 4QPM leads to increased errors on the centroid measurement and larger dispersion of the final pointings. Moreover, in the case of CDR model, we note that the dispersion barely changes when performing TA at 1000, 750, or 500 mas. However, when getting too close to the 4QPM, not only does that lead to a large offset, but it also increases the dispersion in the final pointings.
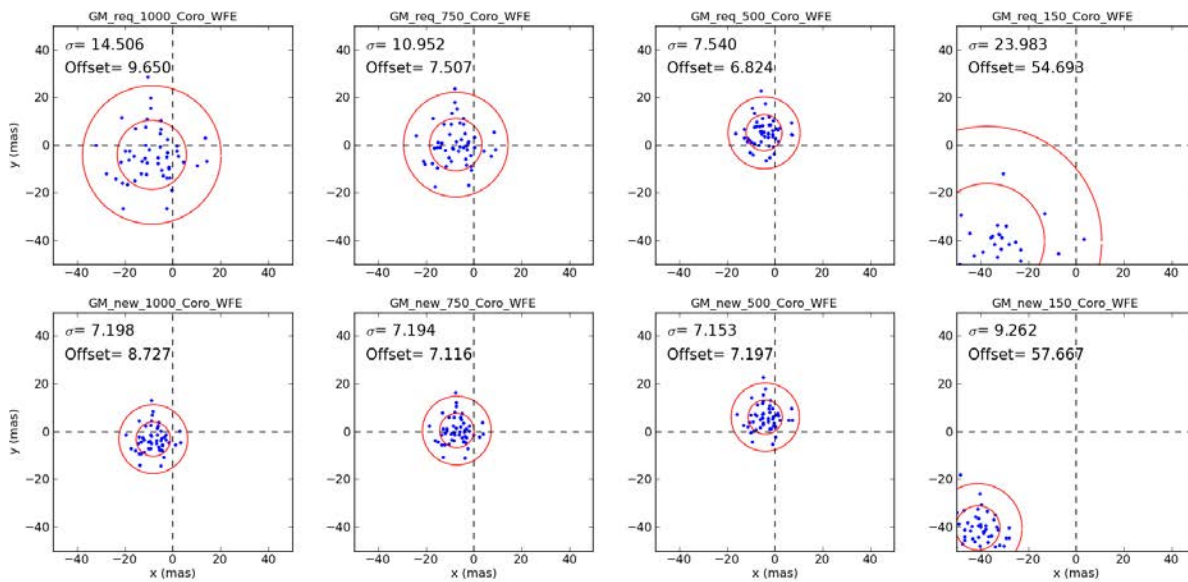
Figure 13: Results for the Single TA scenario using the Requirement (top row) and CDR (bottom row) slew accuracy models for different intermediate positions. From left to right, the intermediate positions are 1000, 750, 500, and 150 mas.

The effect of slew accuracy for larger slews is also observed for the Requirement slew accuracy model, where the dispersion increases as we go further out, whereas the dispersion and the offset remain practically unchanged for the CDR model (see also **Error! Reference source not found.**). Both the requirement model at 500 mas and the CDR model in general achieve similar levels of performances. Based on these results, the Single TA scenario becomes appealing for many reasons: (1) the dispersion is close to the coronagraphic requirements of 5 mas radial, (2) similar

performances can be achieved for different slew accuracy models, which alleviates some of the dependence on the latter, and (3) only one acquisition is necessary, which has implications on time and mechanism uses for MIRI.

5.3   Twin TA

The Twin TA scenario uses mirrored images across the 4QPM center from which a simple average of the two centroids is done to decrease the symmetric adverse effect of the 4QPM on the PSF. The procedure requires only two acquisitions and simple onboard arithmetics. Results are presented in **Error! Reference source not found.** for both the Requirement and CDR slew accuracy models (top and bottom rows respectively).
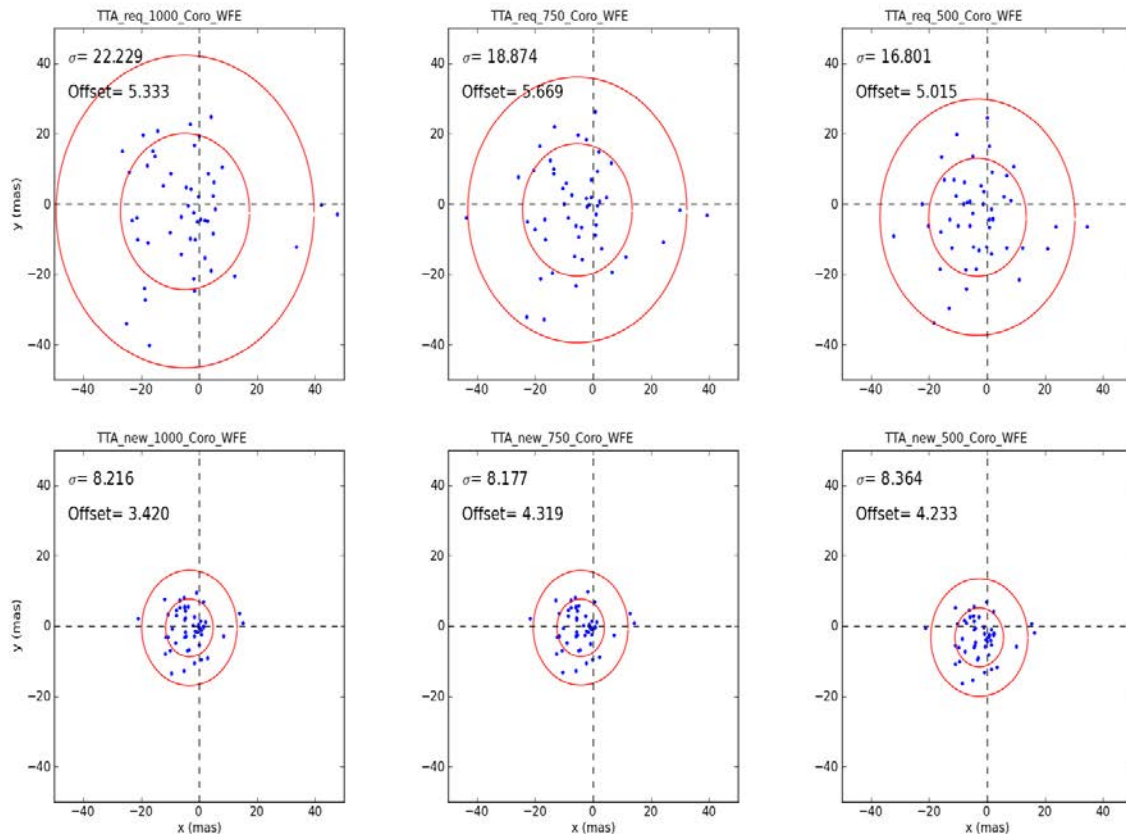
Figure 14 Results for the Twin TA scenario using the Requirement (*top row*) and (*bottom row*) models at different intermediate positions. From left to right, 1000, 750 and 500 mas.

Again, the effect of the slew accuracy is obvious between the Requirement and CDR slew models. However, unlike the Single TA scenario, we do not observe similar performances at smaller intermediate positions (e.g. 500 mas). Moreover, the dispersion of the final pointings is consistently larger than the Single TA scenario by ~15%, although the mean offsets are consistently smaller by a factor ~2. These smaller mean offsets are likely a result of our mirrored approach, which averages out some of the distortion of the PSF due to the 4QPM.

5.4   Quad TA

For the Quad TA, we use two patterns, as illustrated in **Error! Reference source not found.**, both of which are designed to average out and minimize the symmetrical effect of the 4QPM on the centroid measurements. We use a square pattern (QTA) and a cross pattern (QTAX) and the results for both, using the Expected slew accuracy model, are presented in **Error! Reference source not found.**. We show the Expected slew accuracy model here because the results are midway between those using the Requirement and CDR slew model.

In general, we find similar trends for both Quad TA scenarios. We again observe the typical behavior for TA: (1) smaller intermediate position with smaller slews leads to tighter final pointings and (2) centroid measurements too close to the 4QPM consistently drives the final pointings off. Despite these trends, the dispersions are generally larger for the Quad TA scenarios than for the Single and Twin TA scenarios, which we attribute to the fact that slewing four times, rather than once or twice, introduces a proportionally larger error in the pointings. The mean offsets, on the other hand, are considerably smaller (factor ~2) than with the Single TA scenario and suggest that multiple acquisitions can help improve the mean offsets. In particular, a significantly smaller offset is observed for QTAX at 750 mas. Finally, even with the CDR slew model, neither Quad TA scenarios can better constrain the dispersion when compared to the Single or Twin TA scenarios.
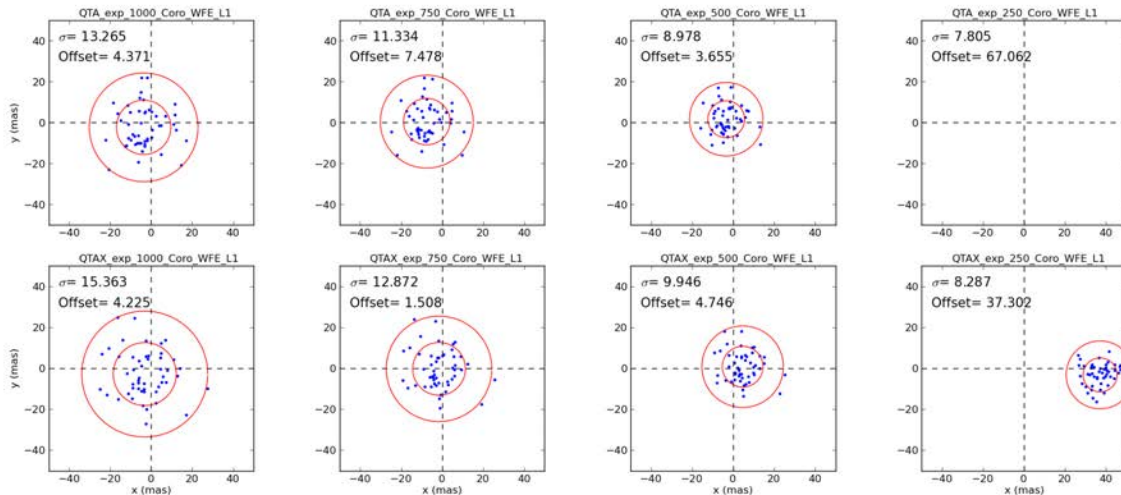
Figure 15 Results for the Quad TA scenarion using the Expected slew accuracy model. We use a square pattern (*top row*) and a cross pattern (*bottom row*) at different intermediate position (1000, 750, 500 and 250 mas from left to right respectively) and a latency of 1%. Note that QTA at 250 mas is offset out of the range of the plot.

These results suggest two alternatives: either we use the scenario that gives the smaller dispersion and find a way to tackle the larger offset or vice versa. On the one hand, using

smaller slew errors leads to tighter final, whereas, on the other hand, scenarios using multiple acquisitions yield smaller offsets. These results are summarized in Figure 16. So, in order to

investigate whether the dispersion in the Twin and Quad TA scenarios can be further decreased, we implemented a small variation in the two scenarios. Instead of simply averaging the four centroids, we compensate every slew by averaging the error of the previous slews. Therefore, for the final slew, we correct the centroid position by averaging the errors on the four previous slews, and slew from this corrected position. In doing so, we are better off using the information at hand (instead of doing a simple average). Although not shown here, the overall results using this variation of the Twin and Quad TA scenarios (we also extended it to Octo TA, which we do not discuss further here) do not show tighter dispersions or smaller, nor any sign of improvement with the number of acquisitions (i.e. 2, 4, and 8).
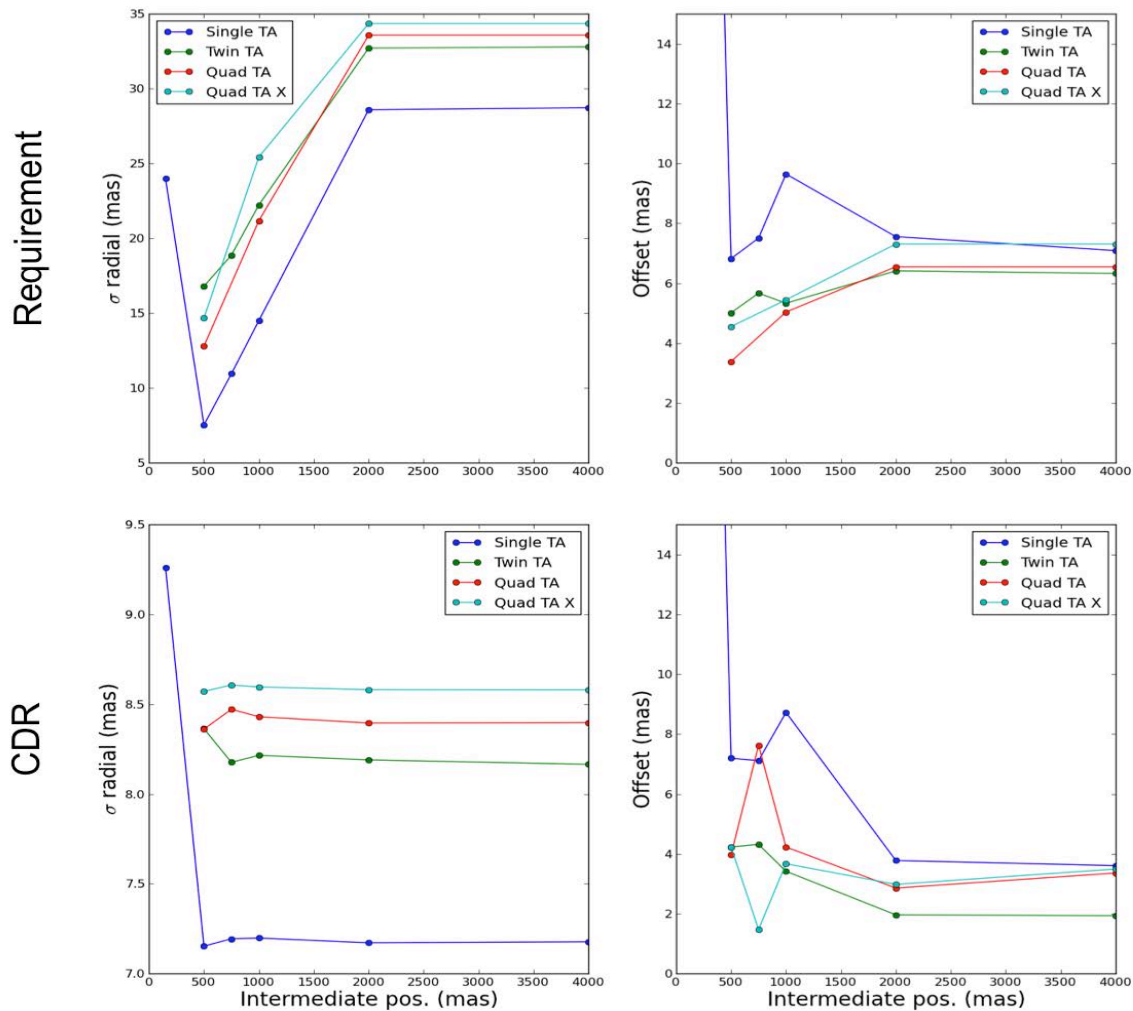
Figure 16: Summary of our simulation results for the requirement (top row) and CDR (bottom row) slew accuracy models. The left panels show the 1-σ dispersion and the right panels show the mean offset, both as a function of intermediate position.

Error! Reference source not found. summarizes our results for all four TA scenarios in Figure 16 and reports their optimal performance given the slew accuracy model used. Considering all

the scenarios and slew accuracy models, we find that Single TA does best in terms of final pointings dispersion, whereas the other three scenarios achieve smaller mean offsets in general. These smaller offsets for the scenarios involving multiple TA confirm that using multiple TA helps averaging out some of the distortion caused by the 4QPM.

Table 1 Summary of out best results for the three slew accuracy models used in this report.

	Optimal position (mas)	Requirement		Expected		CDR model	
		σ_r	Offset	σ_r	Offset	σ_r	Offset
Single TA	500	8	7	6	7	7	7
Twin TA	500	17	5	11	4	8	4
Quad TA	500	13	4	9	4	8	4
Quad TA X	750	20	2	13	2	9	2
Iterative TA	N/A	---	---	6	15	2*	16*

*The Iterative TA scenario with the CDR slew model includes FSM slews

6 Target Acquisition at 15.50 μm

We now perform simulations at longer wavelength (15.5 μm) to assess the dependence of TA on wavelength. **Error! Reference source not found.** shows the PSF of a 5800 K blackbody through the 4QPM and neutral density filter (FND) for all three masks (designed for 10.65, 11.40, and 15.50 μm). It is clear from **Error! Reference source not found.** that the 4QPM at 15.50 μm introduces much less distortion in the PSF than at shorter wavelengths. Assuming a Rayleigh-Jeans spectrum for the star, the fraction of the flux at 15.5 μm is much smaller than at 10.65 μm, and therefore the overall impact of the FQPM on the PSF shape with the FND is more negligible at 15.5 μm than at 10.65 μm. Note that in the case of unresolved hot dust (e.g. asteroid-belt type), or for other astrophysical objects (e.g. quasars), the shape of the spectrum could be completely different from a Rayleigh-Jeans shape and our result would not apply. Future simulations would be needed to assess the impact of combined astrophysical sources on the TA process. On the other hand, the effect of the 4QPM on the PSF at 10.65 μm and 11.40 μm is very similar, so we do not expect a significant impact on the TA between these two wavelengths.
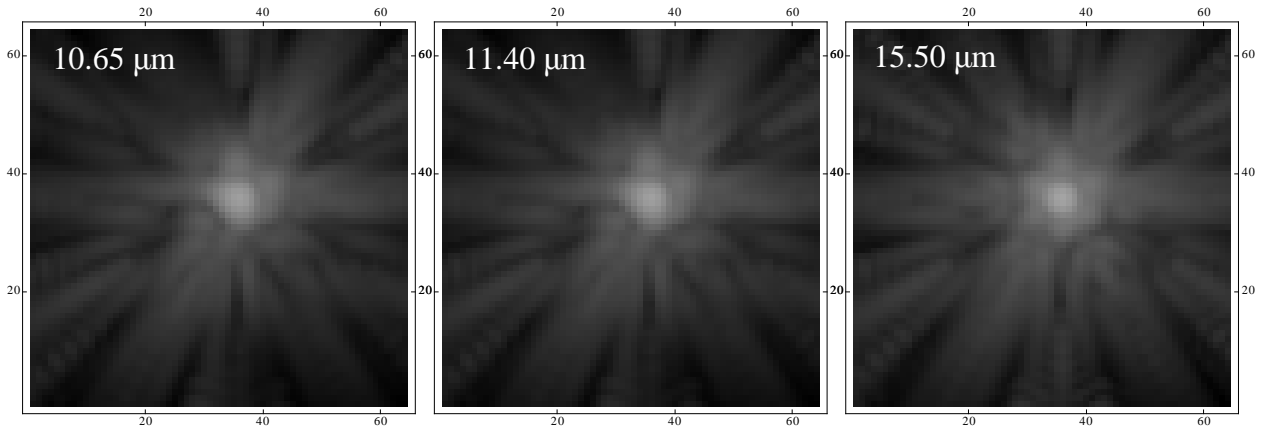
Figure 17 PSF through the neutral density filter and 4QPM at different wavelengths. The PSF is offset by ~500 mas at 45 degrees on the 4QPM and the units are in pixels.

The results of TA at different wavelengths and under different scenarios are summarized and compared to our results at 11.40 μm in **Error! Reference source not found.** and **Error! Reference source not found.** (for the Requirement and the CDR slew accuracy models respectively). Despite the larger and almost undistorted PSF at 15.50 μm (for a Solar-type spectrum), we see that TA accuracy is not affected by using a longer wavelength compared with that achieved at shorter wavelengths. In particular, the dispersion of the final pointings remains the same at both wavelengths, although we do observe a trend towards smaller offsets at longer wavelengths. Once again, however, the main limiting factor in positioning the star as close to the center of the 4QPM as possible is the slew accuracy, as illustrated in **Error! Reference source not found.**. These results demonstrate that the same optimal scenario applies to all three masks and that we will be able to perform TA equally well with all three 4QPM.
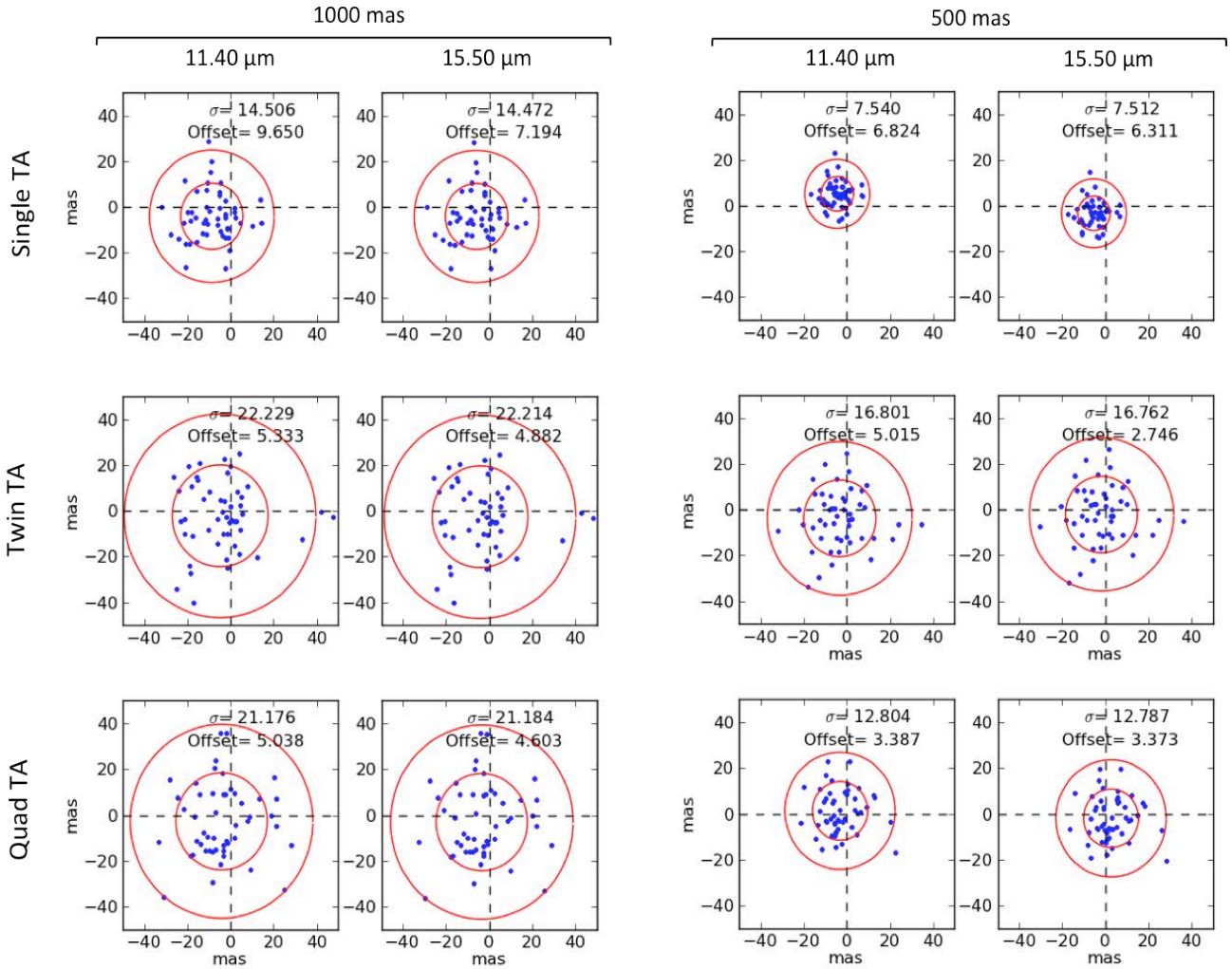
Figure 18 Comparison of TA at 11:40 µm and 15.50 µm for different intermediate position (1000 and 500 mas) a different TA sections. The top, middle and bottom rows are for the Single, Twin and Quad Scenarios, respectively. All are modeled with wavefront error and the Requirements slew accuracy model.
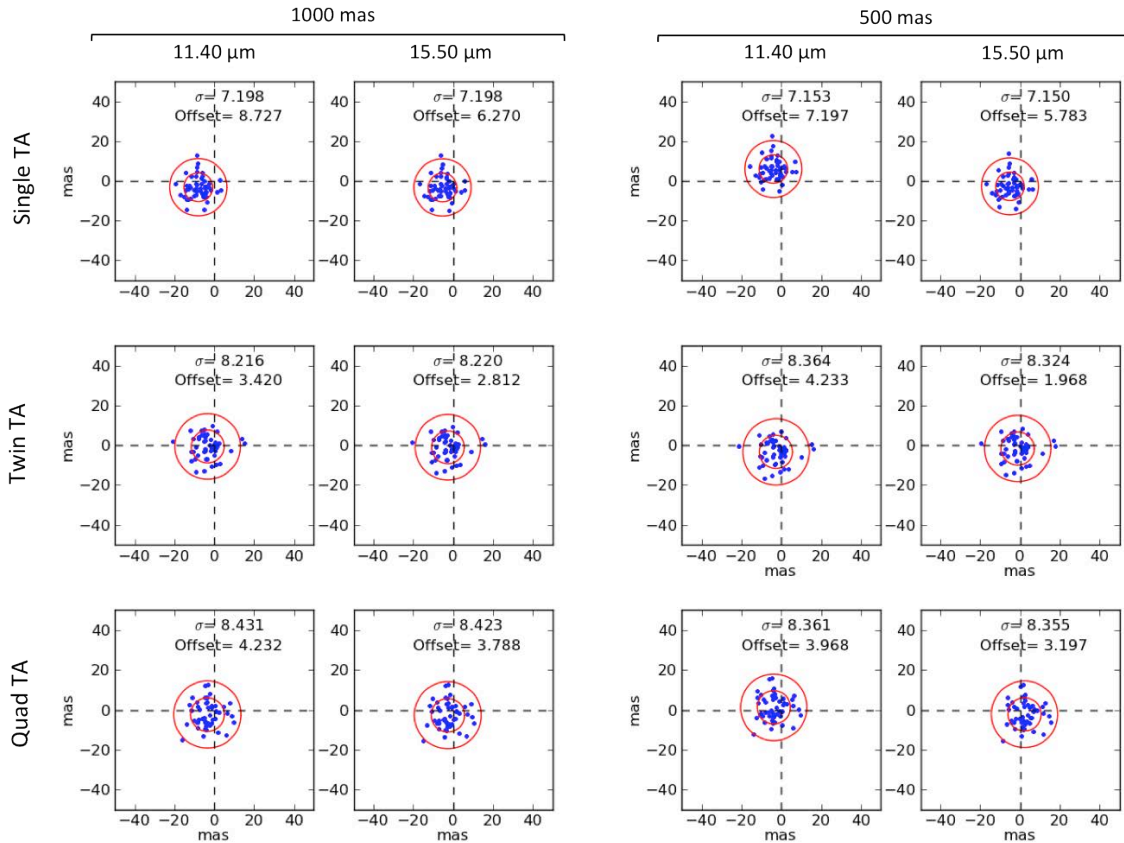
Figure 19 Same as Figure 18 but for the CDR slew accuracy model

7   PSF higher-order moments

In order to further constrain the exact position of the star on the 4QPM and to potentially help predict the next slew, we investigate the PSF higher-order moments. As of now, only the second-order moments (x^2 and y^2) are coded in the centroid algorithm (see Meixner et al. 2007) but we nevertheless use higher-order mixed moments to assess their potential usefulness.
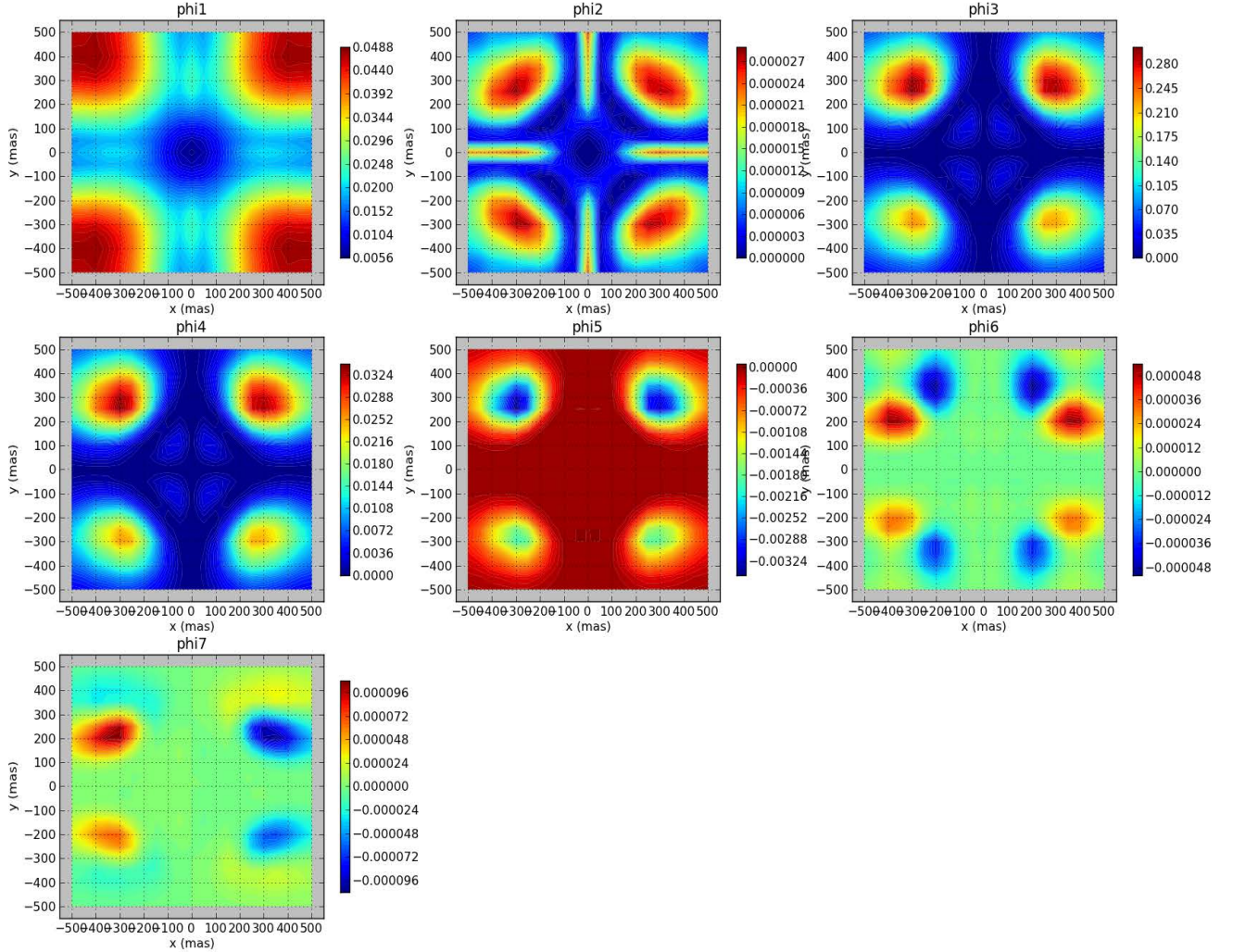
Figure 20 PSF invariant moments at 11.40 μm without wavefront error.

The central moments are defined as follows:

$$\mu_{pq} = \sum_{x} \sum_{y} (x - \bar{x})^p (y - \bar{y})^q f(x, y)$$

where $\bar{x}$ and $\bar{y}$ are the coordinates of the centroid and $f(x, y)$ is the image value at (x, y). A combination of the second- and third-order central moments can yield a set of moments that are invariant under translation, rotation, and scaling (ϕ_1 to ϕ_7; see Gonzalez & Woods 2001 for more details), which we show in **Error! Reference source not found.** for the 11.40 μm 4QPM without wavefront error. Note that despite using invariant form of the moments, our simulations show that they are in fact not quite invariant, mainly because of small numerical differences in the PSF as a function of position on the 4QPM.
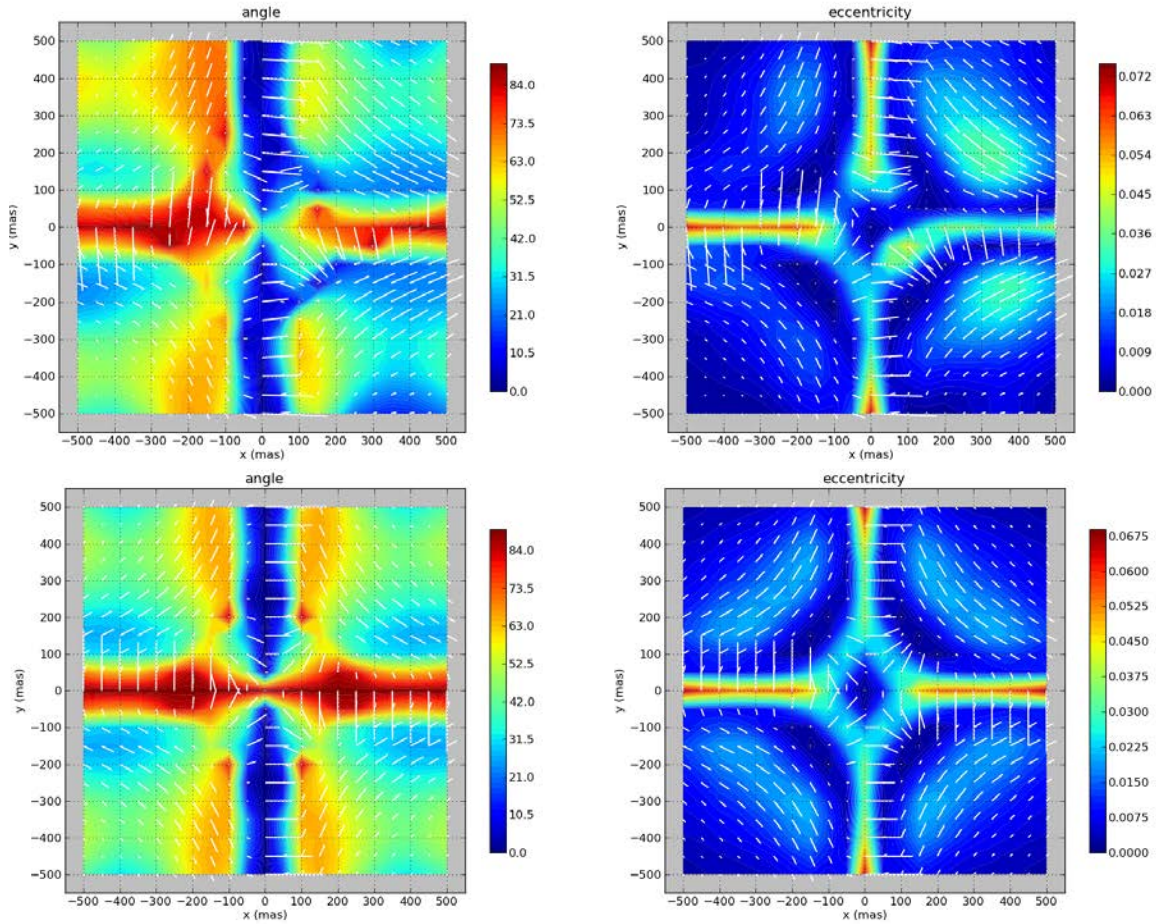
Figure 21: PSF major axis angle with respect to the x-axis (left) and eccentricity (right) with and without wavefront error (top and bottom rows respectively). The lines show the orientation of the major axis and their length is proportional to the eccentricity. The maps are both at 11.40 μm.

The range of values for each of these moments is relatively small (less than one order of magnitude) and therefore makes these moments rather insensitive to position on the 4QPM. These small numbers also most likely explain the (small) asymmetries seen in the moments despite not using any wavefront error. Most importantly, degeneracy over the 4QPM in all the moments is such that no unique position can be derived from any combination of moments, therefore limiting the use of moments in pinpointing the position of the star on the 4QPM.

Figure 21 on the other hand shows a combination of the second order moments (x^2, y^2, and xy) to quantify the *shape* of the PSF for the cases with and without wavefront error (top and bottom rows respectively). The right panels show the eccentricity of the PSF while the left panels show the angle of the major axis with respect to the x-axis. The (pseudo-) vectors show the orientation of the major axis and their length is proportional to the eccentricity. Again, these shape parameters show degeneracy and no unique orientation and/or eccentricity can help pinpoint the position of the star on the 4QPM. We therefore conclude that the use of the orientation of the PSF's major axis *only* to constrain the direction of the next slew seems unreliable.

8   Summary & Conclusions

We presented the results from a large set of simulations of target acquisition (TA) under MIRI's 4QPM coronagraphic modes. We investigated the effects of the 4QPM, the observatory's slew accuracy, image latency, noise, wavelength, and various scenarios on the dispersion and offset of the final pointings. Overall, the effects of latency, noise, and wavelength were shown to be negligible, whereas the intermediate centroid position during TA had a stronger effect on the final pointings. In general, we find that the dispersion can be tightened if fewer slews are used (as well the CDR model with a smaller error) whereas the offset can be decreased by a factor of ~2 by performing multiple symmetric acquisitions around the center of the 4QPM. In particular, we showed that an intermediate position smaller than ~500 mas is too close to the center of the 4QPM and that the error introduced in the TA procedure leads to a larger dispersion and offset of the final pointings. Some of the scenarios investigated here marginally meet the coronagraphic pointing requirement if interpreted at the one-sigma level, assuming the CDR pointing model and no additional error sources in the pointing system (e,g, transients and drifts, which we assumed are corrected by the current upgrade to the pointing system).

As for the different scenarios investigated, our main findings were as follow:

1.   the current optimal TA, which comes closest to the requirements, is the Single TA at a 500-mas intermediate position. However, we caution that performing TA at such small separations can impose small but non-negligible latents on science images (e.g. planets) and should be further investigated.
2.   the Single TA and Iterative TA scenarios both yield the smallest dispersions of final pointings, although the mean offset is above the requirement.
3.   the QTAX and Iterative TA scenarios both yield the smallest offsets although the dispersion is larger.
4.   these results hold true when using the CDR slew accuracy model (and in some cases, the Expected slew accuracy model).

Our results also show that target acquisition as far out as 4" is possible if the slew accuracy remains small (~4 mas or smaller) for slews as large as 4". Such a TA strategy (i.e. at large distances) is appealing since it would significantly decrease the amount of latency, if any, in the science images. Our results also demonstrate once more that the accuracy with which we can position a star on the 4QPM depends on (and is mostly limited by) the slew accuracy. If the CDR pointing performance is not achieved, the current TA scenarios do not meet the coronagraphic pointing requirements. However, in this case, we suggest that one possible avenue to mitigate some of the TA issues is to use small dithers under fine guidance and more advanced data processing techniques (see Soummer 2012).

Finally, our investigation of the PSF higher-order moments suggests that the moments (or any combinations of moments) might not be sensitive enough to unambiguously pinpoint the location of the star or give us a good lever on direction of the next slew. We see no benefits in using high-order PSF moments and therefore recommend not implementing them for TA purposes.

9   References

Cavarroc, C., Boccaletti, A., Baudoz, P., & Regan, M. 2008, PASP, 120, 1016-1027

Gonzalez, R.C. & Woods, R.E. 2001, *Digital Image Processing 2nd Edition*, Prentice Hall, New Jersey

Gordon, K., & Meixner M. 2008, STScI Technical Report, JWST-STScI-001407, SM-12

Meixner, M., Cavarroc, C., Regan, M., & Boccaletti, A. 2008, STScI Technical Memorandum, JWST-STScI-0001134

Soummer, R., & Makidon R. 2010, STScI Technical Report, JWST-STScI-001952, SM-12

Soummer, R., Hines, D., & Marshall, P. 2012, STScI Technical Report, submitted (JWST-STScI-003058, SM12)

Soummer, R. 2012, STScI Technical Report, submitted (JWST-STScI-003059, SM12)